Analysis of Recurrent Patterns in Toroidal Magnetic Fields

Allen R. Sanderson, *Member, IEEE,* Guoning Chen, *Member, IEEE,* Xavier Tricoche, *Member, IEEE,*
David Pugmire, Scott Kruger, and Joshua Breslau

Abstract—In the development of magnetic confinement fusion which will potentially be a future source for low cost power, physicists must be able to analyze the magnetic field that confines the burning plasma. While the magnetic field can be described as a vector field, traditional techniques for analyzing the field's topology cannot be used because of its Hamiltonian nature. In this paper we describe a technique developed as a collaboration between physicists and computer scientists that determines the topology of a toroidal magnetic field using fieldlines with near minimal lengths. More specifically, we analyze the Poincaré map of the sampled fieldlines in a Poincaré section including identifying *critical points* and other topological features of interest to physicists. The technique has been deployed into an interactive parallel visualization tool which physicists are using to gain new insight into simulations of magnetically confined burning plasmas.

Index Terms—Confined magnetic fusion, magnetic field visualization, Poincaré map, periodic magnetic fieldlines, recurrent patterns.

---

1 INTRODUCTION

The development of magnetic confinement fusion which will potentially be a future source for low cost power is an important research area. Physicists are particularly interested in using magnetic fields to confine the burning plasma in a toroidal shaped device known as a *tokamak* (Figure 1a). To achieve stable plasma equilibrium, the fieldlines of these magnetic fields need to travel around the torus in a helical fashion (Figure 1a). This helical behavior can be accomplished by summing up a toroidal field traveling in the torus around the center of the torus with a poloidal field moving in circles orthogonal to the toroidal field. In order to design such efficient reactors, physicists must be able to analyze the magnetic fields from numerical simulations and characterize their orbits. Note that the magnetic fields confined in a tokamak theoretically are in the form of divergence free vector fields and as described below whose fieldlines have a periodic, quasi-periodic, or chaotic behavior (Section 3.3). Whether the magnetic field remains divergence free numerically depends on the choice of the representation in a particular code and the error introduced through numerical simulation.

The symplectic, and in particular area preserving nature of the corresponding flow mapping makes existing analysis techniques difficult to apply because rather involved numerical schemes are required for their accurate study [22]. Indeed, typical techniques are applied to non-symplectic vector fields, such as fluid flows, or in scenarios where ensuring the divergence-free nature of the flow is not of paramount importance. In those cases, the main features of interest can be identified with standard numerical techniques in simple data representations. Nonetheless, recent work [25, 26] has started to investigate the specific benefits of enforcing the divergence-free nature of the data interpolation to achieve the long term numerical stability of streamline-based visualizations in fluid dynamics applications.

To tackle the visualization and analysis of a magnetic field, a

---

- *Allen R. Sanderson is with the Scientific Computing and Imaging Institute, University of Utah, e-mail: allen@sci.utah.edu.*
- *Guoning Chen is with the Scientific Computing and Imaging Institute, University of Utah, e-mail: chengu@sci.utah.edu.*
- *Xavier Tricoche is with Purdue University, e-mail: xmt@purdue.edu.*
- *David Pugmire is with Oak Ridge National Laboratory, e-mail: pugmire@ornl.ogv.*
- *Scott Kruger is with Tech-X Corporation, e-mail: kruger@txcorp.com.*
- *Joshua Breslau is with Princeton Plasma Physics Laboratory, e-mail: jbreslau@pppl.gov.*

Poincaré map is used. The Poincaré map's main feature is that it offers a principled dimensionality reduction to study Hamiltonian systems [23]. The map is formed by the intersection of fieldlines with a plane perpendicular to the axis of the torus (Figure 1b), whereby a sufficient number of intersections ("puncture points") are collected in order to reveal salient patterns in the Poincaré section [20]. These patterns can then be used to characterize the orbits and refine the analysis.

Among all the fieldlines in a toroidal magnetic field, physicists are most interested in the fieldlines that are periodic or quasi-periodic. This interest is because these fieldlines help one understand plasma transport in magnetic fusion research. We briefly describe these fieldlines with more detail in Section 3.3. A periodic fieldline is closed in a finite length and resides on a *rational surface*. Whereas a quasi-periodic fieldline travels over an *irrational surface* given an infinite amount of time. When viewed in the Poincaré section a quasi-periodic fieldline will form one of two distinct structures: a single closed curved (*flux surface*) and multiple closed curves (*island chains*). In between them is the *separatrix* that separates the two structures. Among them, an island chain is the result of the break-up of a rational surface subject to the magnetic perturbation which indicates the reduction in magnetic confinement and hence the plasma burning is less effective. The computation of the Poincaré map of the sampled fieldlines should provide sufficient information on the behavior of the magnetic field and help extract the topological structure of the field by identifying the patterns in the Poincaré plot.

In this paper, we exploit the physical and geometric properties of the toroidal magnetic fieldlines to derive efficient algorithms for constructing Poincaré plots as well as characterizing the topological structures of magnetic fieldlines using a near minimal number of puncture points. The methods presented in this work are purely geometric, local in nature, and geared for parallel computations. Emphasis is on robustness and computational efficiency while ensuring reliable results for visual analysis. The algorithms have been implemented as a library which can be directly integrated into existing visualization software, such as VisIt [2] and SCIRun [1] or be directly used in simulation codes. More specifically, this work has made the following contributions.

- We present efficient algorithms to compute the Poincaré map of the sampled fieldlines in a toroidal magnetic field with a near minimal number of puncture points. This near minimization is achieved by properly computing the toroidal and poloidal winding numbers (i.e. rational periods). This analysis greatly reduces the number of integration steps for each fieldline and leads to a fast computation. In addition, we show that these points are sufficient to recover the important patterns in a Poincaré plot, including flux surfaces and island chains.

- Rather than rely on a dense set of discrete points to represent the

Fig. 1.   (a) Profile of the DIII-D Tokamak and a single quasi-periodic magnetic fieldline (the red curves). (b) The corresponding Poincaré plot for the magnetic fieldline in (a) using 200 puncture points.

pattern formed in Poincaré plot we present a contiguous representation by properly connecting a near minimal set of puncture points. This contiguous representation has helped the physicists identify various magnetic surfaces in an efficient manner. Other smaller features, such as *islands within islands* which were previously difficult to detect, can be identified as well.

- Besides characterizing different magnetic fieldlines, we present the algorithm for extracting the critical points *in* the Poincaré map. They correspond to the fieldlines whose sum of the poloidal magnetic field vanishes (zero magnetic flux). Together with the detected surfaces, they provide the topological information of the given magnetic fields.

- We have applied the present techniques to a number of simulations of the toroidal magnetic fields. The results demonstrate the efficacy of the proposed techniques.

2   RELATED WORK

As noted in the previous section, magnetic fields are described in terms of vector fields. While a rich body of visualization research has focused on the extraction of features of interest in vector fields [28], the relevance of vortices [14, 30, 15, 32], flow separation [16], or shock waves [21] is limited in the context of magnetic fields.

Because of the dynamical nature of toroidal magnetic fields, feature extraction techniques for dynamical systems are relevant to this work [11]. These techniques extract the topological features from the flow, then construct the representative topological graph for visualization [12, 37, 13, 41, 38, 18, 4, 5]. This process involves the extraction of singularities (or critical points) [40, 27, 33, 34] and periodic orbits [42, 43, 44, 39, 4]. However, because the magnetic fields inside a tokamak are typically singularity-free we focus on the work of periodic orbit extraction. A more detailed survey of the analysis techniques for general vector fields can be found in [28, 19].

Within the fusion community researchers have located periodic fieldlines using numerical approaches such as those by [8]. However, these methods are computationally expensive and lack robustness, especially in the complicated geometries of modern experiments. Wischgoll and Scheuermann were the first in the visualization community to present an algorithm for detecting periodic orbits in planar flows [42]. Their method examines how a fieldline re-enters a cell and re-connects. They have also extended their technique to 3D vector fields [43] and time-dependent flows [44]. In the meantime, Theisel et al. [39] presented a mesh independent approach to compute periodic orbits. Recently, Chen et al. [4] proposed a novel and efficient algorithm to extract periodic orbits from surface flows using *Morse decompositions*. However, all of this work requires that the closed orbits attract or repel neighboring streamlines (i.e., hyperbolicity) which is typically *not* the case in toroidal magnetic fields which are divergence free. Therefore, the existing work can not be directly applied.

It is also worth noting the work of Löffelmann et al. [20] who integrated 2D Poincaré plots with the original 3D flow for visualization purposes. However, their data contained synthetic periodic vector fields where the period was known. Recently, an analysis technique for divergence free flow fields has also been proposed by Peikert and Saldo [25, 26] who introduced a divergence cleaning scheme to study vortex breakdown flow patterns through their long-term Poincaré plot. Impressive results were achieved by this method. Note that we did not incorporate it in our implementation because its application would have required a resampling of the computational mesh along with a computational overhead during the integration. Others have used a graph-based approach and machine learning techniques to classify the fieldlines [3]. However, in order to obtain a reasonable accuracy a large number, e.g. $2000 - 2500$ of puncture points per fieldline were necessary. Obtaining this many points requires a large number of integration steps which is not only expensive but also prone to numerical inaccuracies that may lead a fieldline to follow an erroneous path. Instead, the present work aims to detect the magnetic features using a near minimal set of puncture points.

3   BACKGROUND

In this section, we briefly review some important concepts of vector fields, the Poincaré map, and toroidal magnetic fields which will be used in the later discussion.

3.1   Vector Fields

Consider a vector field V on a manifold $\mathcal{M}$, which can be expressed as an ordinary differential equation $\frac{dx}{dt} = V(x)$. The set of solutions to it gives rise to a *flow* on $\mathcal{M}$; that is a continuous function (or map) $\varphi : \mathbb{R} \times \mathcal{M} \to \mathcal{M}$ satisfying $\varphi(0,x) = x, \forall x \in \mathcal{M}$ and $\frac{d\varphi}{dt}\Big|_{t,x} = V(\varphi(t,x)), \forall t \in \mathbb{R}$. A fieldline (or trajectory) through a point $x_0 \in \mathcal{M}$ is a curve on $\mathcal{M}$ corresponding to $x(\cdot) \equiv \varphi(\cdot, x_0)$. Particularly, a fieldline through $x_0 \in \mathcal{M}$ is a periodic orbit if $x(T) = x_0$ for some $T \in \mathbb{R}$ and $T \neq 0$. A periodic orbit is an *invariant set*. A set $S \subset \mathcal{M}$ is called *invariant* if it is transported onto itself by the flow, in other words if $\varphi(t,S) \subseteq S, \forall t \in \mathbb{R}$. In the following, we resort to the conventional Poincaré map to analyze the invariant sets of magnetic fields in plasma confinement and propose a number of novel techniques to assist this analysis.

3.2   Poincaré Map

Let Γ be an orbit (integral curve) of φ in a n dimensional manifold $\mathcal{M}$ (e.g. in our case $n = 3$). Let $\mathcal{S}$ be a cross section of dimension $n - 1$ (e.g. in our case a plane that is perpendicular to the major axis of the torus) such that φ is everywhere transverse to $\mathcal{S}$. $\mathcal{S}$ is known as a Poincaré section. An intersection of Γ with $\mathcal{S}$ is referred to as a *puncture point*, denoted by $p_i \in \mathcal{S} \cap \Gamma$ ($i \in \mathbb{N}$ indicates the ordering of the intersections). The Poincaré map, or *the first return* is defined as a mapping in $\mathcal{S}$ $P : \mathbb{R} \times \mathcal{S} \to \mathcal{S}$ that leads a puncture point p_i to the next position p_{i+1} following an orbit Γ where $p_i, p_{i+1} \in \mathcal{S} \cap \Gamma$. That is, $p_{i+1} = P(p_i) = \varphi(\tau, p_i)$ where $\tau \in \mathbb{R}$ and $\tau > 0$ is the time that has passed when Γ travels from p_i to p_{i+1}. Figure 2 illustrates this concept. All of the puncture points, p_i give rise to the *Poincaré plot* of Γ. A Poincaré map is a well defined method for studying recurrent flows near periodic solutions in a dynamical system.

3.3   Toroidal Magnetic Fields

As introduced previously, the magnetic fieldlines contained in a toroidal device exhibit helical behavior. That is, the fieldline will wind around both the major (toroidal) and minor (poloidal) circles of the torus (Figure 2). A key property characterizing the behavior of a fieldline in a magnetic field is its *safety factor*, q which is the number of times a fieldline goes around the toroidal circle for each rotation around the poloidal circle. The safety-factor is known as such because the value gives an indication of the stability of the plasma confined by the magnetic field. Specifically, a low safety factor indicates better stability. The safety factor of a fieldline can be defined as:

$$q = \lim_{n_T \to \infty} \frac{n_T}{\#_\theta(n_T)} \tag{1}$$

where n_T is the toroidal winding number, i.e. the number of the crossings of a fieldline Γ through a poloidal cross section $\mathcal{S}$ and $\#_\theta(n_T)$ is the poloidal winding number, i.e. the number of crossing of Γ through the toroidal cross section at $z = 0$. In particular, we denote the poloidal winding number as $\#_\theta(n_T)$ when Γ passes through the poloidal cross section n_T times (Figure 2) . Excluding the case of chaotic fieldlines, such a limit exists for a given fieldline.
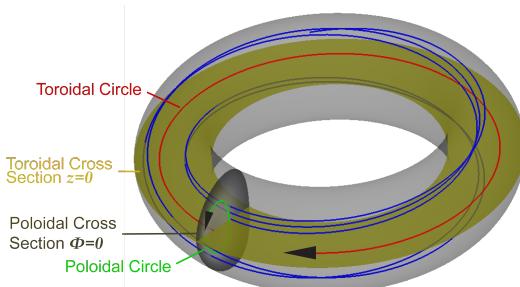
Fig. 2. A magnetic fieldline (blue) that intersects the poloidal plane (gray) and the toroidal plane (gold).

An irrational q implies that the fieldline is quasi-periodic. Such a fieldline lies on an *irrational surface* and spreads out over it. Such surfaces have two types of topology when viewed in a Poincaré section, a single closed curve (Figure3a) or multiple closed curves (Figure 3b). See also Figure 4b. A single closed curve typically represents a magnetic flux surface which when sufficiently perturbed tends to break up into stochastic, space-filling fieldlines. Multiple closed curves represent a magnetic island chain that is the result of the break up of a *rational surface* and are usually associated with a reduction in magnetic confinement (Figure 4b). The number of islands within a chain is equal to the toroidal winding number.

A rational q implies that the fieldline is periodic (or closed in finite distance). Such a fieldline lies on a *rational surface* but does not spread out over it (Figure 3c). Such surfaces are important because a low-order rational q, where the poloidal winding number is small, are the first surfaces to break up into island chains in response to magnetic perturbations.
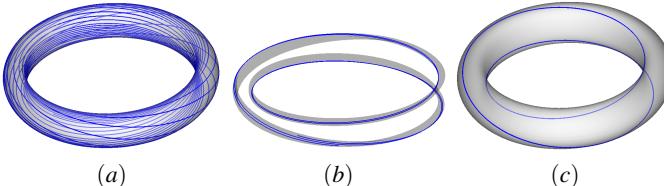
Fig. 3. The quasi-periodic fieldlines that spreads out over an irrational surface: (a) a flux surface, (b) an island chain. (c) A periodic fieldline that traverses a rational surface.

Island chains are of interest because they are locations of instability within the magnetic field. Of particular interest within the island chains are the locations were there is no magnetic flux (aka critical points) [9]. At these locations the poloidal magnetic field vanishes (zero magnetic flux) and a fieldline Γ becomes periodic or closed such that a puncture point at p_i on the Poincaré section is equal to a puncture point at p_{i+n_T}. Where n_T is the fieldline's toroidal winding number. Puncture points $\{p_i, p_{i+1}, ..., p_{i+n_T}\}$ are critical points (Figure 4a). For a rigorous mathematical definition the reader is referred to the work of Greene [9, 10].

There are two types of critical points for a magnetic island chain, commonly referred to as X (saddle) and O (center) points. In the case of an O Point, it is located at the magnetic center of an island. While for an X point, it is located where two flux surfaces appear to cross and form a *separatrix* around the magnetic islands (Figure 4b). The O points represent stable orbits: start a fieldline at a point infinitesimally removed from an O point and a closed surface is formed that surrounds

the point and remains close to it. While the X points represent unstable orbits; a fieldline started at a point infinitesimally removed from an X point will converge exponentially to the point along two of the axes leading in and diverge exponentially along the other two. There are n_T X and O points respectively for each magnetic island chain.

(a) $\qquad\qquad (b)$
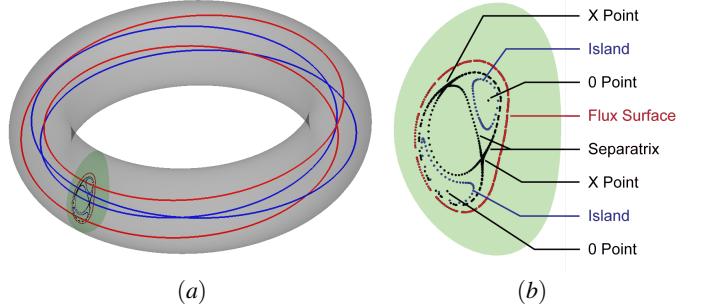
Fig. 4. (a) Two periodic fieldlines originating from an island chain's O point (red) and X Point (blue). (b) A Poincaré plot showing a flux surface (red), an island chain with two islands (blue) and their associated O points (black), and the separatrix (black).

4 OVERVIEW

The basic idea of this work is to make use of the Poincaré map to analyze the toroidal magnetic fields. The Poincaré plot is computed from a number of fieldlines seeded at different locations. For each fieldline, we compute its first N puncture points on the Poincaré section. Second, we compute the toroidal and poloidal winding numbers of this fieldline according to the information associated with each puncture point (Section 5). A second approach based on a ridgeline plot is used to calculate and verify the poloidal winding number (Section 7). Once computed and verified, the winding numbers are then used to extract the topology of the magnetic field. This includes the characterization of fieldlines (Section 6) and the extraction of critical points (Section 8). Finally, the puncture points are properly connected based on the previous analysis to provide a contiguous representation for the physicists to interpret (Section 9).

5 PUNCTURE POINTS AND WINDING NUMBERS

The first step is to collect a set of puncture points from the Poincaré section while counting the number of associated toroidal and poloidal windings of the fieldline. Let P_i be a tuple describing the state of each puncture point of a fieldline Γ with the Poincaré section $\mathcal{S}$. Further, let $P_i = (p_i, n_i, m_i)$ where p_i represents the position of P_i in $\mathcal{S}$, n_i is the number of crossing of Γ through $\mathcal{S}$ when reaching p_i (including the seed point), and m_i the number of crossing of Γ through the toroidal cross section when $d(\Gamma)_z > 0$ (increasing z coordinates) and when reaching p_i. We start from $P_0 = (p_0, 1, 0)$. Each time, Γ intersects with $\mathcal{S}$, $n_i = n_i + 1$. Similarly, $m_i = m_i + 1$ when Γ intersects the toroidal cross section. This crossing can be easily identified by examining the sign changes of the z coordinates of the integration points of Γ. Because we record this crossing information only at P_i, there could be multiple crossings of Γ through the toroidal cross section between P_i and P_{i+1}. This iteration continues until the end of fieldline Γ is reached.

The toroidal winding number is then found for a value of T such that:

$$\min_{T \in \mathbb{N}}(d) = \sum_{i=T} \left\| (P_{i+T}(m_{i+T}) - P_i(m_i)) - (P_i(m_i) - P_{i-T}(m_{i-T})) \right\| \quad (2)$$

is minimized, where $P_i(m_i)$ returns the number of crossings of Γ through the toroidal cross section plane when reaching the puncture point P_i. When d is minimized, the toroidal winding number $n_T = T$ and the poloidal winding number $\#_\theta(n_T) = P_{n_T}(m_{n_T})$.

The minimization is based on an important observation: for a given toroidal winding number n_T, the poloidal winding number should be consistent between every n_T puncture points. For example, if the toroidal winding number is 5 and the poloidal winding number is 2. Then the poloidal winding counts, m_i could be:

$$0, 1, 1, 1, 2, \quad 2, 3, 3, 3, 4, \quad 4, 5, 5, 5, 6$$

In this case the difference between every 5th value (the toroidal winding number) is 2 (the poloidal winding number).

Once the toroidal and poloidal winding numbers have been determined the safety factor for a magnetic surface or its fieldline is typically referred as a ratio of the two winding numbers, e.g. a 5,2 surface.

6 FIELDLINE CLASSIFICATION

After determining the toroidal winding number n_T, it is possible to classify the fieldline as being periodic, quasi-periodic, or chaotic. The first step of classifying a fieldline is to group its associated puncture points into n_T "winding groups" where winding group j contains puncture points $(p_j, p_{j+n_T}, p_{j+2*n_T}, p_{j+3*n_T}, ...)$

When a fieldline is periodic, the puncture points within a winding group will be coincident. That is $p_j = p_{j+n_T} = p_{j+2*n_T} = p_{j+3*n_T} = ...$. However, to account for numerical inaccuracies a user defined factor, typically based on the fieldline integration step size, δ is introduced such that two points are coincident when $\|p_j - p_{j+n_T}\| < \delta$.

When a fieldline is quasi-periodic, the puncture points, when connected (as described below) will form one of two topologies: a single closed curve (a flux surface) or multiple closed curves (an island chain), as shown in Figure 4b. For a flux surface the single closed surface will be composed of exactly n_T sections, one section for each winding group. While for an island chain there will be exactly n_T islands, again one for each winding group.

Island chains can be distinguished from flux surfaces using three simple tests. First, for an island chain, the centroid, C of the puncture point set will lie on the outside of the boundary of each individual winding group (i.e. an island). Whereas for a flux surface, the centroid, C will lie inside of its boundary. This observation holds when the magnetic field is not under large perturbations. However, it has not been extensively tested under highly stochastic conditions.

Second, in an island chain, with each island composed of k connected points, a change in direction of the point connections of an island can be observed relative to the centroid, C from above. This situation can be detected by examining the cross-product of the vectors formed by the points C, p_0, and p_1 which would be in the opposite direction to the cross-product of the vector formed by points C, $p_{k/2}$, and $p_{k/2+1}$ whereas for a flux surface the cross products would be in the same direction. This difference is demonstrated in Figure 5.
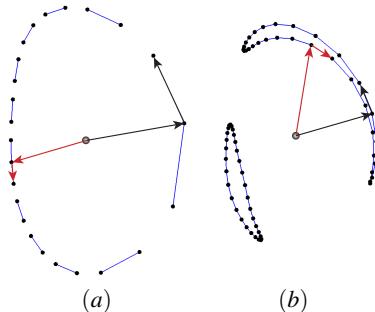
Fig. 5. (a) Poincaré section of a 11,5 flux surface showing two pairs of vectors whose cross products are both in the same direction relative to the centroid. (b) Poincaré section of a 2,1 island chain showing two pairs of vectors whose cross products are in opposite directions relative to the centroid.

The final component comes from the observation that for a flux surface puncture points when connected from one winding group will overlap the connected puncture points in a neighboring winding group.

Whereas for an island chain the puncture points when connected will overlap themselves. This observation is fully discussed in Section 9.

The puncture points of fieldlines are tested against these observations for consistency. Those fieldlines that are found consistent are classified as being on either a flux surface or an island chain; otherwise they are classified as being chaotic.

7 RIDGELINE PLOT

While the method in Section 5 for determining the poloidal winding number provides accurate results, it is not the only measure that is available to ascertain it. As a verification of the previous computation, we observed that the fundamental period of a *ridgeline plot* of a local maximum for each fieldline is proportional to the poloidal winding number. If this proportionality is consistent then we are able to verify that the correct poloidal winding number was obtained. Otherwise, we return the inconsistency to the user for further investigation. We also note that in the case of an island chain the fundamental period is proportional to the number of points along the boundary, Section 9.

7.1 Ridgeline Formation

For each poloidal winding in the fieldline there is a local maximum, r with respect to the toroidal cross section (i.e the $Z = 0$ plane), which is defined as:

$$\Gamma_z(r) > 0; \frac{\partial \Gamma(r)}{\partial z} = 0. \tag{3}$$

The *ridgeline plot* is defined as the collection of these local maxima.

To visually construct the ridgeline plot, the cylindrical coordinate system is used to transform the torus into a cylinder (Figure 6). The periodic nature of the fieldline is then apparent. However, it is not the periodicity of the fieldline itself that is of interest but the periodicity of the maximal points as defined in Equation (3). Utilizing multiple integration steps to extend the fieldline, maximal points were extracted and used to construct a ridgeline plot (Figure 7). The oscillation of the ridgeline can be attributed to an area preserving deformation of the magnetic surface as the field line precesses around it. For an island chain the oscillation is further influenced by the rotation of the islands between each poloidal section.
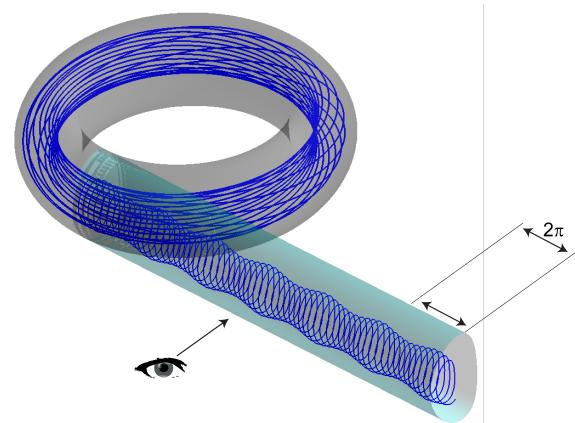
Fig. 6. The original toroidal geometry containing a single fieldline for multiple toroidal windings in Cartesian coordinates superimposed with the same geometry in Cylindrical coordinates. This transformation changes the torus (gray) into a cylinder (blue) and removes the toroidal component of the fieldline.

7.2 Fundamental period

The most basic approach to determine the fundamental period of the ridgeline plot is to use Time-Domain methods such as zero-crossing rate (ZCR), autocorrelation, and Yin estimators [7]. While ZCR techniques are simple to implement they succumb to the problem of multiple events per cycle which occurs with magnetic island chains.
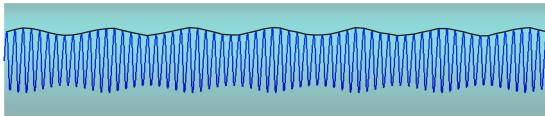
Fig. 7. The same fieldline in Figure 6 in cylindrical coordinates viewed perpendicular to the longitudinal axis of the cylinder. The ridgeline plot of maximal points is shown in black and has a period of 10.

Another option is to use autocorrelation to measure the similarity in the ridgeline waves but it too can suffer when higher harmonics are present. Instead a Yin Estimator was used and is similar to autocorrelation except that it attempts to minimize the following difference:

$$\min_{f \in \mathbb{N}}(\sigma) = \sum_{i=0} (r_i - r_{i+f})^2 \tag{4}$$

where r_i are the local maxima as in Eq. 3, and f is the *fundamental period* (or fundamental frequency). When analyzing a flux surface $f \propto \#_\theta(n_T)$ (Figures 8a and 9a). While for an island chain $f \propto \#_\theta(n_T) * M$ where M is the number of points along the boundary of one island in the chain (Figures 8b and 9b). Figure 9a shows that the fundamental period could be an integer multiple of the poloidal winding number and occurs when the number of ridgeline points is greater than four times the poloidal winding. However, there are special cases such as islands within islands (Section 12) where integer multiples truly exist. These cases are currently under further investigation.
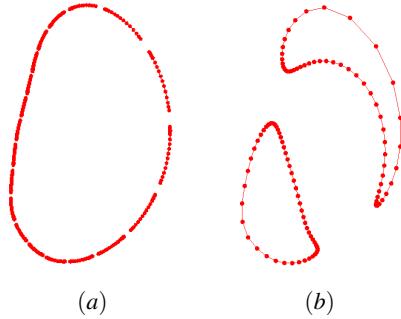
Fig. 8. (a) Poincaré section of a 19,10 flux surface. The number of curved sections, 19 corresponds to the toroidal winding number. (b) Poincaré section of a 2,1 island chain. The number of islands, 2 corresponds to the toroidal winding number. Each island contains 53 puncture points which corresponds to the fundamental period of the ridgeline plot.
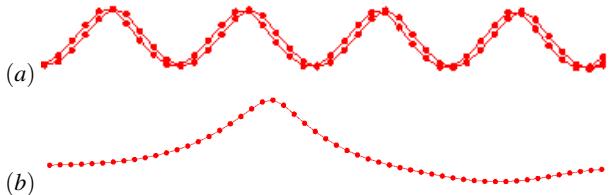
Fig. 9. (a) Ridgeline plot for the 19,10 flux surface with a fundamental period of 40. This plot illustrates that the fundamental period can be an integer multiple of the poloidal winding number. (b) Ridgeline plot for the 2,1 island chain with a fundamental period of 53 matching the number of puncture points that define one island. For both plots two sections of the ridgeline have been overlapped. For the flux surface ridgeline had a variance of 3.63e-03 while the island chain the ridgelines are almost exact having a variance of 1.24e-06.

8 EXTRACTING O POINTS AND X POINTS

When a magnetic surface has been identified topologically as an island chain, we wish to find the critical points (O and X points) associated

with it. Finding the X and O points is important to physicists because in contrast to Computational Fluid Dynamics (CFD), Magneto-hydrodynamics (MHD) has even greater sensitivity to the locations of critical points due to the description of the magnetic fields. By finding these critical points and the resultant change in topology, a better understanding of the underlying dynamics can be achieved.

Numerically searching for the O points is done by performing an iterative search until a fieldline becomes periodic using the following criteria:

Given the toroidal winding number n_T, and for each $i \in \{0,..,n_T - 1\}$ a fieldline is periodic when: $p_i = p_{i+n_T} \pm \delta$, where δ is a user defined factor to account for numerical inaccuracies. This definition is the same one used to define a rational fieldline. However, a fieldline crossing a critical point does not lie on a surface.

We note that an O point is located near the geometric center of an island. As the cross-sectional area of an island goes to zero (i.e. as the poloidal magnetic field vanishes) the geometric center converges to the O point. To compute the geometric center of an island, we find the straight line skeleton [36]. For an object such as an island the skeleton is but a cord. The mid point of the cord is the approximate geometric center (aka the maximal interior point). If the fieldline becomes periodic at the geometric center then the O point is known. If not, the geometric center defines another, albeit smaller nested magnetic island whose geometric center is then iteratively tested (Figure 10).

Determining the X points is much simpler as we can take advantage of the symmetry. For some of the toroidal magnetic fields we are currently investigating, each X point is the reflection of an O point of the same island chain with respect to the $Z-$axis of the Poincaré plane. As such, the locations of the X points are the mirror opposite of the O points. However, when this symmetry is not present a general solution will be required and is on going research.
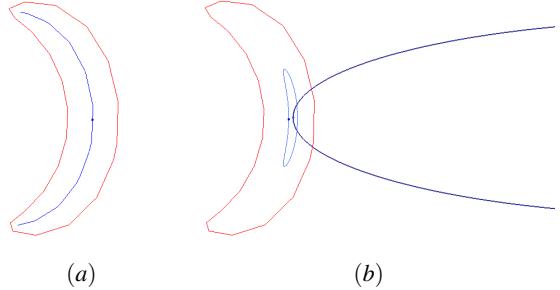
Fig. 10. (a) A 1,1 Island chain along with its straight line skeleton and mid cord point approximating the geometric center. (b) The same island using the geometric center to define another island (blue) with its geometric center defining the O Point as shown by the magnetic fieldline that is periodic.

9 CONNECTING THE PUNCTURE POINTS

Determining both the toroidal and poloidal winding numbers is important not just for determining a fieldline's safety factor and whether it is rational or irrational but it also allows the puncture points to be used to visualize a linear approximation of the cross-section of the magnetic surface. As previously discussed, the existing simulation and visualization tools simply generate a dense set of puncture points and relies on the user's eyes to form a contiguous representation.

Instead, it is possible to connect the puncture points to form a contiguous representation. As previously noted, for each surface with a toroidal winding number of n_T, the puncture points are placed into n_T winding groups. The points in each group can be connected into a contiguous curve. While the points within a winding group are contiguous, the groups are not. That is, winding group j is not adjacent to winding group $j + 1$. Knowing the neighboring group is necessary for terminating connections within a group so that overlaps do not occur. The neighboring group is determined by the toroidal and poloidal winding numbers and the Blankinship algorithm:

$$s * \#_\theta(n_T) = 1 \ (mod \ n_T) \qquad (5)$$

such that winding groups j and $j + s$ are neighbors. To connect the puncture points the following steps are taken:

1) Number the successive puncture points p_i of the fieldline.

2) For a given toroidal winding number n_T, and for each $i \in \{0,..,n_T - 1\}$, connect the points $\{p_i, p_{i+n_T}, p_{i+2n_T}, ...\}$ to produce n_T piecewise linear segments.

3) Connect points until a segment of one winding group overlaps either a segment from a neighboring winding group, or itself.

This algorithm is illustrated in Figure 11 for a 2,1 flux surface.
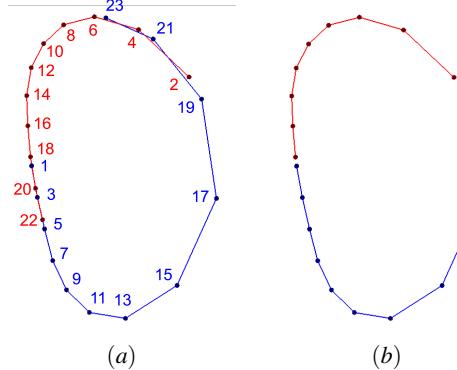
Fig. 11. (a) The puncture points of a 2,1 flux surface with the points numbered based on their puncture order. (b) The same surface in (a) after trimming the overlapping segments.

Traditionally a Poincaré plot consists of the intersections of approximately, 50 to 100 fieldlines with 1000 to 3000 puncture points per fieldline. Besides the heavy computation, the resulting clutter makes the task of identifying the resulting structures very difficult.

For instance, in Figure 12, a fieldline with a safety factor of 8,3 that intersects the Poincaré section 32 times is shown. In isolation the structure is clear. A second example is shown in Figure 13 for a fieldline with a safety factor of 5,2 that intersects the Poincaré section 105 times. In this case, it is difficult to discern that the points form five distinct structures (an island chain) until they are connected. In Figure 14a we combine the Poincaré plots from Figures 12a and 13a. It is not until the segments are connected that the structure becomes clear.

For Figures 12b and 13b each curve is numbered based on its winding group ordering which is determined based on the ordering of the puncture points. This numbering gives another visual representation of the relationship of the toroidal and poloidal windings. For instance, for a toroidal winding number of n_T there are n_T winding groups. Further, if one traverses the winding groups in order, one will trace around the poloidal plane $\#_\theta(n_T)$ (the poloidal number) times.

10 NEAR MINIMAL SET OF PUNCTURE POINTS

One of the difficulties in constructing a Poincaré Plot is determining the number of puncture points needed. Too few points will lead to insufficient information for fieldline classification, while too many points will waste computational resources. For example, a fieldline on the outboard side of the torus will require more integration steps to generate the same number of puncture points as will a fieldline on the inboard side of the torus. Further, the closer a fieldline is to a rational surface (i.e. being periodic) the less it will spread out over the surface and thus require more puncture points to fully define the cross-section of the surface.

To find a near optimal set of puncture points, it is necessary to generate enough points so that when connecting puncture points, a single overlap can be achieved between segments from one winding group to another. Or, in the case of an island chain, the segments within a winding group overlap. This process is described as Step 3 of the algorithm in Section 9. If no overlap is found more puncture points are generated until one is found. The following provides the algorithm:
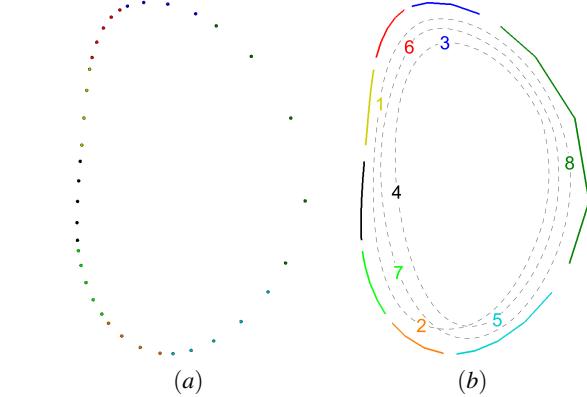
Fig. 12. The Poincaré plots of a 8,3 flux surface using (a) the original 32 points (b) the contiguous representation based on a toroidal winding number of 8. Tracing around the poloidal plane from winding group to winding group reveals the poloidal winding number of 3.
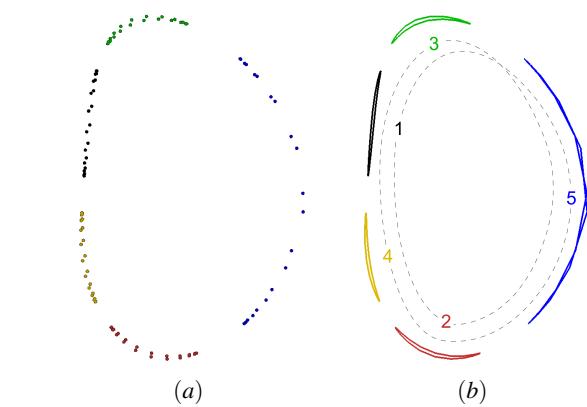
Fig. 13. The Poincaré plots of a 5,2 island chain using (a) the original 105 points (b) the points connected based on the toroidal winding number 5. Tracing around the poloidal plane from island to island reveals the poloidal winding number of 2
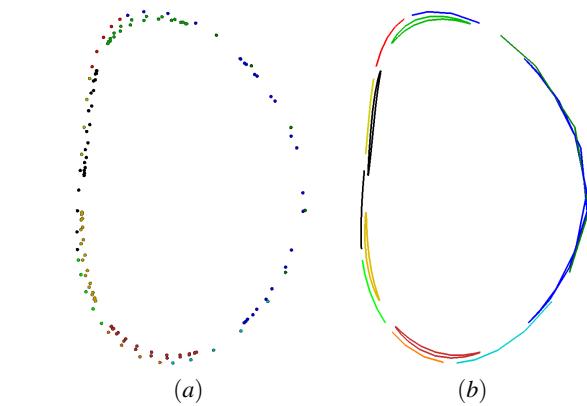
Fig. 14. The Poincaré plots showing the surface and island chain from Figures 12 and 13 using (a) point-based representation (b) our contiguous representation. The structure of the two fields is not obvious until the points are connected in a contiguous manner.

1) Test for an overlapping section, if one is found, stop.

2) For the current winding group, determine the length, l of the last segment.

3) Determine the length, L between the segment in 2) and the first point in the neighboring winding group,

4) The approximate number of the required additional puncture points is L/l.

Because the length, L is a cord length rather than the arc length which

is unknown, the number of additional points will be under-estimated. This under-estimation is the reason for the iterative process.

While theoretically this approach should produce a minimal number of puncture points, in practice it does not. This is because the segment lengths, l are not a constant but a function of their location in the cross-section. Therefore, the approach actually produces a near minimal number of puncture points.

It should be noted that while the above is sufficient for completing the cross-section, additional puncture points may be required for performing the ridgeline plot analysis. For a flux surface the analysis will require $2 \times \#_\theta(n_T)$ puncture points while an island chain will require $2 \times M \times \#_\theta(n_T)$ puncture points where M is the number of points along the boundary, (Section 7).

11 DEPLOYMENT

One of the goals of the project was to create an analysis tool that could be used for interactively creating visualizations. In order to create a complete view of the magnetic field, it may be necessary to compute up to a thousand fieldlines. Integral methods for computing these fieldlines can be very expensive, especially because we wish to maintain the divergence-free nature of the field. For details on the integration methods used the reader is referred to [35, 6].

Because the computation of each individual streamline is an independent calculation, parallelization is an effective method for reducing the overall amount of work. The resources required for fieldline computation are a function of four basic parameters: 1) size of the data set, 2) the number of initial seed points, 3) the spatial distribution of the seed points and 4) the complexity of the magnetic field.

In cases where the entire data set can fit into main memory, parallelization becomes trivial. The fieldlines are divided among the set of processors, each processor loads the data set into memory, and the integrations are performed in parallel. When the data set is too large to fit into main memory, several parallelization strategies may be used, depending on the nature of the data sets and the initial seed points. The first is to parallelize across fieldlines. The fieldlines are divided among the set of processors, and each processor will perform the required I/O to integrate through the data set to completion. A second technique is to parallelize across the data set. Each processor is assigned a subset of the data set, and individual fieldlines are passed from processor to processor as it traverses through the data set. These first two techniques can be subject to significant imbalance, depending on the four basic parameters mentioned above. Parallelization across fieldlines can become the I/O bottleneck if the fieldlines traverse through large portions of the dataset, particularly if the vector field is cyclical, as is the case here. Parallelization across the data set can lead to processor load imbalance if the fieldlines are spatially concentrated in certain regions of the data set. To alleviate this imbalance, a third parallelization strategy is made available to the user, a hybrid parallelization technique that dynamically adapts the strategies based on processor utilization. With this hybrid strategy, a balance between redundant I/O and streamline communication is sought that maximizes processor utilization. Complete details of this implementation can be found in [29].

12 RESULTS AND DISCUSSION

Before presenting the results we summarize the complete analysis steps:

1) Generate a field line requesting N poloidal puncture points per fieldline (for our cases N is typically 50), Section 11. 2) Determine the winding numbers using the puncture points, Section 5. 3) Determine the poloidal period using the ridgeline points, Section 7. 4) Classify the field line as either an island chain, flux surface, rational surface, or chaotic, Section 6. 5) Based on the current analysis determine if more puncture points are needed. If not, connect the points into a contiguous curve, Section 9; otherwise, request more points and repeat the analysis, Section 10. 6) For an island chain iteratively search for the critical points, Section 8.

We now present results obtained in conjunction with our collaborators who are working on the development of magneto-hydrodynamic

(MHD) solvers. Each example shown here is based on the user manually selecting seed points for the fieldlines. Typically 50 seed points along the z=0 axis (a line segment across the Poincaré section) are selected. Manual selection of the seeds may result in features such as thin higher order island chains being missed. However, they are of less interest than lower order island chains that grow during the simulation. That said, our technique would benefit from a numerical search being performed between the initial seeds to ensure that the majority of the features are found.

The first example is from SIESTA which is an ideal MHD 3D-equilibrium solver, capable of dealing with magnetic islands and stochastic regions [31]. This MHD solver is an ideal candidate because of the specific interest of the physicists in looking at island formation. In Figure 15a, we show a typical Poincaré plot that has been used for analysis. The magnetic field contains three island chains: A 1,1 island chain (green) that is obvious, an outer 2,1 island chain (blue) that is visible but hard to fully disambiguate, and 17,10 island chain that can not be seen due to its small size. In Figure 15b, we show the same Poincaré plot using a near minimal set of puncture points that have been connected in a contiguous manner. This connectivity makes the topology of the magnetic field immediately obvious. Further, the island identification technique has been used to detect the smallest 17,10 island chain. This chain is so small that the dots cover each island. Previously, such islands would not be seen until they are more fully developed later in the simulation. As such, our collaborators can follow island formation and development much easier, which is an important part of their research.

M3D (Multi-level 3D) is another MHD solver that has been used for nonlinear studies of plasmas in tokamaks, stellarators, and other devices [24]. Figure 16 shows a puncture plot of the magnetic field in an early stage of a nonlinear simulation of a *sawtooth crash* in the CDX-U tokamak. The magnetic field has become unstable resulting in the exponential growth of a 1,1 island. In Figure 16b the island can be seen clearly as a thin blue crescent. This set represents the hot core of the plasma, and has begun magnetically reconnecting with the outer set at the X-point (not shown) which is poloidally opposite to the O-point of the island. Figure 18 shows a step in the later time in the sequence during which the *sawtooth crash* is well underway. A significant portion of the original inner region has reconnected across the X-point (which is now on the mid-plane on the right), resulting both in substantial growth of the 1,1 island, which will soon replace the original central region as the new magnetic axis; and, correspondingly, in substantial mixing of the hot core plasma with cooler plasma from the outer region, flattening the plasma temperature profile. This flattening greatly reduces the fusion rate, so our collaborators would like to learn how to avoid these modes.

In the next example, our collaborators have used NIMROD [35] which is a non-ideal magneto-hydrodynamics with rotation simulation code. Figure 17 shows a Poincaré plot of the magnetic field mid way through the time sequence of a simulation of a major *disruption* of an experimental run of the DIII-D tokamak [17]. At this point of time, two 2,1 island chains have formed. In Figure 17b both island chains can be clearly seen and marks the beginning of energy loss within the core. Figure 19 shows a time later in the sequence during which the *disruption* is well underway. The islands continue to grow and the core region becomes largely stochastic as due to the lack of any structure (the puncture points from fieldlines that are chaotic are currently not displayed).

One of the most unique topological cases is when islands form within islands which is a result of the island surface breaking up. In this case, the puncture points for a single island do not form a contiguous boundary but instead form islands. Figure 20 shows an island chain that is composed of three islands. Each island contains six smaller islands (zoom-in view of Figure 20). The detection of such self-similarity is done by recursively using the technique described in Section 6. What would normally be classified as a flux surface becomes an island, and what would normally be classified as an island chain becomes islands within islands. These small scale topological features are an example of stochastic behavior within the magnetic
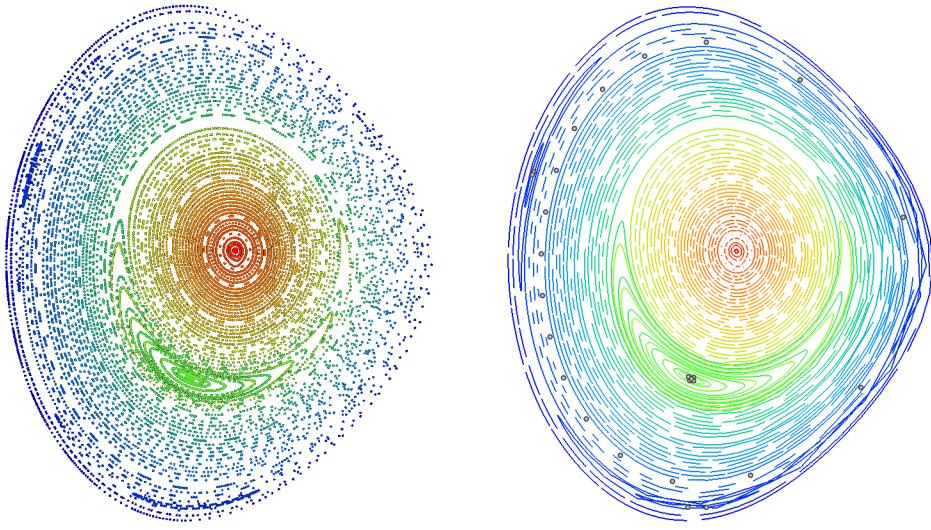
Fig. 15. (a) A Poincaré plot of a Siesta MHD simulation with 75 fieldlines. Each fieldline computes 200 puncture points. (b) The same plot using a near minimal number of puncture points that have been connected. There is a small 17,10 island chain (17 grey dots) that has been identified and can not be recognized in (a). In both images, the points and lines are color based on their safety factors.
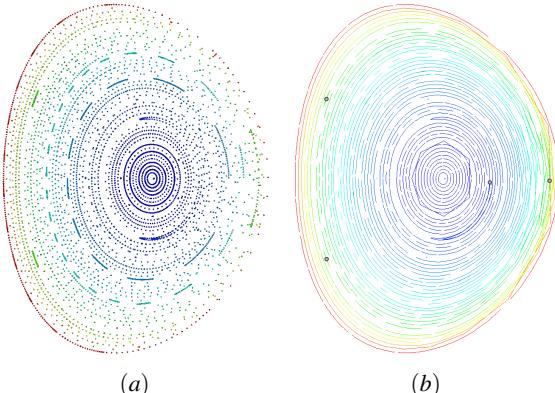
Fig. 16. The Poincaré plots of a magnetic field from M3D. There are two thin island chains, one green and one blue, that are difficult to see (a) until the points are connected and the islands identified (b).
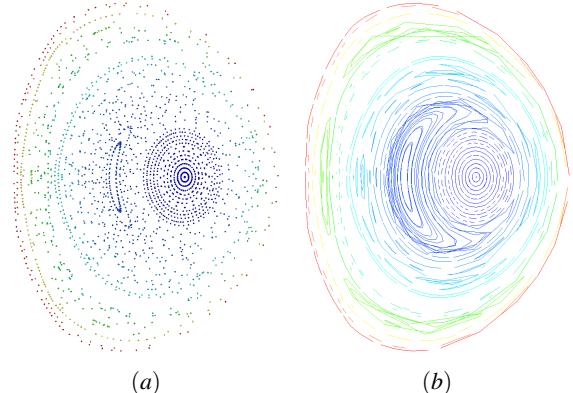
Fig. 18. A Poincaré plot of the same magnetic field in Figure 16 but later in the simulation where the growth of the island chains is much more pronounced.
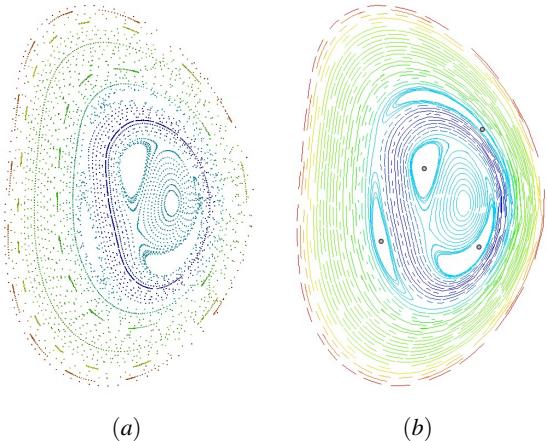
Fig. 17. The Poincaré plots of a magnetic field from NIMROD. While the inner island chain can be seen on the point based plot (a) the outer island chain is not clearly visible until the points are connected in a contiguous fashion (b).
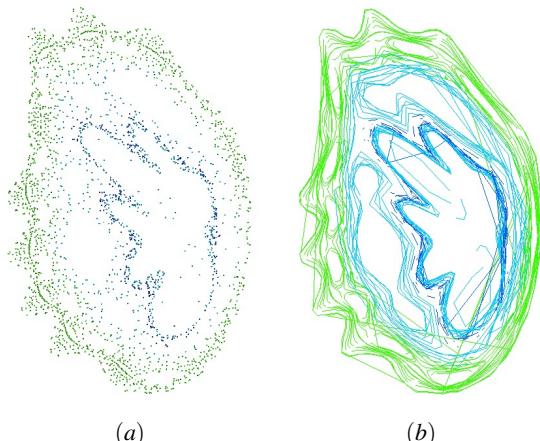
Fig. 19. A Poincaré plot of same magnetic field in Figure 17 but later in the simulation where the growth of the island chains is much more pronounced. It is difficult to discern the structure on the point based plot (a) compared to contiguous plot (b).

field. Traditional techniques for discovering such topological features are rarely used because of the computational expense.
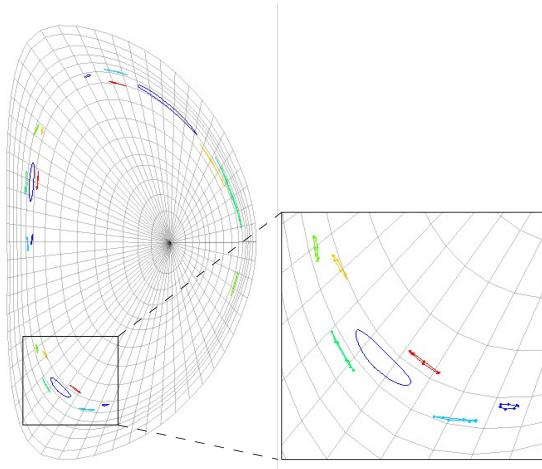
Fig. 20. (left) Poincaré Plot showing a 3,1 island chain that is composed of six islands within itself - aka islands within islands. (right) a closeup of one set of islands within islands. For reference, a sibling island chain is shown (blue) nested within the six islands within islands.

In the final example (Figure 21) we show the power of our tool in that not only can they be used to construct the 2D Poincaré plot but they can also be used to visualize the complexities of the 3D structure of the magnetic surface. While such visualizations are not typically used by physicists as part of their daily analysis, they are extremely useful for educational purposes and for creating presentation quality visualizations. Figure 22 provides another example where the Poincaré plot has been combined with a 3D magnetic surface (green) along with multiple iso-temperature surfaces to create a complete visualization.
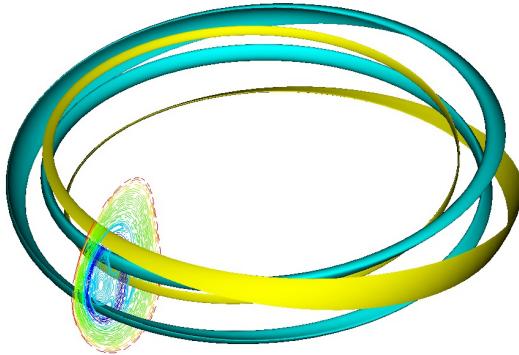
Fig. 21. Two surfaces from two 2,1 magnetic island chains shown in 3D overlay with the corresponding Poincaré Plot. Each surface can be considered as a Möbius strip that has been folded on top of itself. The surfaces shows the complexity of the magnetic field in 3D.

13 CONCLUSIONS AND FUTURE WORK

We have presented the application of a geometric technique to the analysis of toroidal magnetic fields which allows for the creation of Poincaré plots using a near minimal set of puncture points. This greatly reduces the computational costs when compared to traditional Poincaré plot generation. We have also proposed efficient algorithms to compute the toroidal and poloidal winding numbers of a fieldline. These two numbers are then used to compute the safety factor of the fieldline, which can be applied to characterize the fieldline into different topological categories. This permits the identification of different
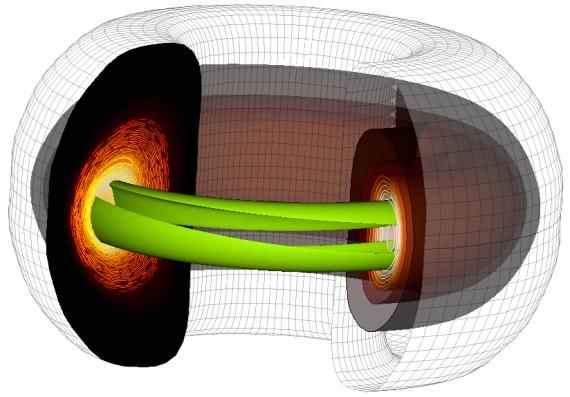
Fig. 22. A complete visualization of a magnetic confinement fusion simulation that highlights a magnetic surface (green) which forms an "island chain", along with a Poincaré plot overlayed on top of a series of transparent iso-temperature surfaces.

magnetic surfaces including the flux surfaces and island chains from the Poincaré plot. Further, the critical points in the plot corresponding to the periodic fieldlines in the magnetic fields are extracted. Combining the extracted flux surfaces, island chains and the critical points, we are able to analyze the topology of the magnetic fields in the form of Poincaré map of the fieldlines. In addition, the discrete puncture points are connected to provide a contiguous representation of the Poincaré map which can more effectively convey the topological information than traditional discrete point-based representations. Finally, we have applied our technique to a number of simulations of a toroidal magnetic field. The results demonstrate the efficacy of our approach.

From the application physicists viewpoint the value added by incorporating the technique into their work flow is that it makes it much quicker, easier, and more efficient to read off the major topological features of the magnetic field by glancing at the enhanced Poincaré plot. At the same time they are able to interactive explore not only the magnetic field but also put the results into context with other scalar and vector data sets such as shown in Figure 22.

However, there are still a number of limitations of the present work. First, our results based on the near minimal set of puncture points have lost the smooth representation of the patterns in the Poincaré plot in some cases. This has led to some artifacts, especially when the fieldlines are sampled close to the wall of the tokamak (i.e., the boundary of the torus). The thin island chains appearing there exhibit the artifact of self-intersection due to the lack of puncture points. Second, the present framework does not handle the chaotic fieldlines which could deliver important information about the magnetic field. Third, the current detection of X points depends on the extraction of O points. It is important to identify them directly and compute the separatices from them, which helps promote this technique to the analysis of more general magnetic fields. Finally, it is interesting to study the behavior of the islands within islands and develop efficient technique to characterize them. We plan to investigate these problems in our future work.

14 ACKNOWLEDGMENTS

REFERENCES

[1] Scirun, http://software.sci.utah.edu/scirun.html.
[2] Visit visualization tool, http://www.llnl.gov/visit/.
[3] A. Bagherjeiran and C. Kamath. Graph-based methods for orbit classification. In *In SIAM International Conference on Data Mining*. SIAM, 2005.

[4] G. Chen, K. Mischaikow, R. S. Laramee, P. Pilarczyk, and E. Zhang. Vector Field Editing and Periodic Orbit Extraction Using Morse Decomposition. *IEEE Transactions on Visualization and Computer Graphics*, 13(4):769–785, Jul./Aug. 2007.

[5] G. Chen, K. Mischaikow, R. S. Laramee, and E. Zhang. Efficient Morse Decompositions of Vector Fields. *IEEE Transactions on Visualization and Computer Graphics*, 14(4):848–862, Jul./Aug. 2008.

[6] J. M. Finn and L. Chacón. Volume preserving integrators for solenoidal fields on a grid. *Phys. Plasmas*, 12(5):054503, 2005.

[7] D. Gerhard. Pitch extraction and fundamental frequency: History and current techniques. Technical report, TR 2003-06.

[8] J. M. Green. Locating three-dimensional roots by a bisection method. *Journal of Computational Physics*, 98:194–198, 1992.

[9] J. M. Greene. Vortex nulls and magnetic nulls. *Topological Fluid Dynamics*, pages 478–484, 1990.

[10] J. M. Greene. Locating three-dimensional roots by a bisection method. *J. Comput. Phys.*, 98(2):194–198, 1992.

[11] J. Hale and H. Kocak. *Dynamics and Bifurcations*. New York: Springer-Verlag, 1991.

[12] J. L. Helman and L. Hesselink. Representation and Display of Vector Field Topology in Fluid Flow Data Sets. *IEEE Computer*, 22(8):27–36, August 1989.

[13] K. M. Janine, J. Bennett, G. Scheuermann, B. Hamann, and K. I. Joy. Topological segmentation in three-dimensional vector fields. *IEEE Transactions on Visualization and Computer Graphics*, 10:198–205, 2004.

[14] J. Jeong and F. Hussain. On the identification of a vortex. *J. Fluid Mechanics*, 285:69–94, 1995.

[15] M. Jiang, R. Machiraju, and D. Thompson. A novel approach to vortex core region detection. In *In Data Visualization 2002. Proc. VisSym'02*, pages 217–225, 202.

[16] D. Kenwright, C. Henze, and C. Levit. Feature extraction of separation and attachment lines. *IEEE Transactions on Visualization and Computer Graphics*, 5(2):135–144, 1999.

[17] S. Kruger, D. Schnack, and C. R. Sovinec. Dynamics of the major disruption of a diii-d plasma. *Phys. Plasmas*, 12:56113, 2005.

[18] R. Laramee, H. Hauser, L. Zhao, and F. H. Post. Topology Based Flow Visualization: The State of the Art. In *Topology-Based Methods in Visualization (Proceedings of Topo-in-Vis 2005)*, Mathematics and Visualization, pages 1–19. Springer, 2007.

[19] R. Laramee, H. Hauser, L. Zhao, and F. H. Post. Topology Based Flow Visualization: The State of the Art. In *Topology-Based Methods in Visualization (Proceedings of Topo-in-Vis 2005)*, Mathematics and Visualization, pages 1–19. Springer, 2007.

[20] H. Löffelmann, T. Kucera, and M. E. Gröller. Visualizing poincare maps together with the underlying flow. In *In International Workshop on Visualization and Mathematics '97*, pages 315–328. Springer-Verlag, 1997.

[21] D. Lovely and R. Haimes. Shock detection from computational fluid dynamics results, 1999.

[22] J. E. Marsden and M. West. Discrete mechanics and variational integrators. *Acta Numerica*, pages 357–514, 2001.

[23] P. J. Morrison. Magnetic field lines, hamiltonian dynamics, and nontwist systems. *Phys. Plasmas*, 7:2279, 2000.

[24] W. Park, E. Belova, G. Fu, X. Tang, H. Strauss, and L. Sugiyama. Plasma simulation studies using multilevel physics models. *Phys. Plasmas*, 6:1796, 1999.

[25] R. Peikert and F. Sadlo. Visualization Methods for Vortex Rings and Vortex Breakdown Bubbles. In A. Y. K. Museth, T. Möller, editor, *Proceedings of the 9th Eurographics/IEEE VGTC Symposium on Visualization (EuroVis'07)*, pages 211–218, May 2007.

[26] R. Peikert and F. Sadlo. Flow topology beyond skeletons: Visualization of features in recirculating flow. In H.-C. Hege, K. Polthier, and G. Scheuermann, editors, *Topology-Based Methods in Visualization II*, pages 145–160. Springer, 2008.

[27] K. Polthier and E. Preuß. Identifying vector fields singularities using a discrete hodge decomposition. In *Mathematical Visualization III*, pages 112–134. Ed: H.C. Hege, K. Polthier, 2003.

[28] F. H. Post, B. Vrolijk, H. Hauser, R. S. Laramee, and H. Doleisch. The State of the Art in Flow Visualization: Feature Extraction and Tracking. *Computer Graphics Forum*, 22(4):775–792, Dec. 2003.

[29] D. Pugmire, H. Childs, C. Garth, S. Ahern, and G. Weber. Scalable computation of streamlines on very large datasets. In *Proceedings of the Conference on High Performance Computing Networking, Storage and Analysis*, November 2009.

[30] M. Roth and R. Peikert. A higher-order method for finding vortex core lines. In *VIS '98: Proceedings of the conference on Visualization '98*, pages 143–150, Los Alamitos, CA, USA, 1998. IEEE Computer Society Press.

[31] R. Sanchez, S. Hirshman, and V. Lynch. Siesta: an scalable island equilibrium solver for toroidal applications. In *American Physical Society, 49th Annual Meeting of the Division of Plasma Physics*, 2007. abstract #GP8.130.

[32] T. Schafhitzel, J. E. Vollrath, J. P. Gois, D. Weiskopf, A. Castelo, and T. Ertl. Topology-preserving λ_2-based vortex core line detection for flow visualization. *Computers & Graphics*, 27(3):1023–1030, 2008.

[33] G. Scheuermann, H. Hagen, H. Krüger, M. Menzel, and A. Rockwood. Visualization of Higher Order Singularities in Vector Fields. In *Proceedings of IEEE Visualization '97*, pages 67–74, Oct. 1997.

[34] G. Scheuermann, H. Krüger, M. Menzel, and A. P. Rockwood. Visualizing nonlinear vector field topology. *IEEE Transactions on Visualization and Computer Graphics*, 4(2):109–116, 1998.

[35] C. Sovinec, D. Barnes, T. Gianakon, A. Glasser, R. Nebel, S. Kruger, D. Schnack, S. Plimpton, A. Tarditi, M. Chu, and the NIMROD Team. Nonlinear magnetohydrodynamics with high-order finite elements. *Journal of Computational Physics*, 195:355, 2004.

[36] M. Tanase and R. C. Veltkamp. Straight line skeleton in linear time, topologically equivalent to the medial axis. In *Proceedings EWCG 2004, 20th European Workshop on Computational Geometry*, pages 185–188, 2004.

[37] H. Theisel, T. Weinkauf, H.-C. Hege, and H.-P. Seidel. Saddle connectors - an approach to visualizing the topological skeleton of complex 3d vector fields. In *VIS '03: Proceedings of the 14th IEEE Visualization 2003 (VIS'03)*, page 30, Washington, DC, USA, 2003. IEEE Computer Society.

[38] H. Theisel, T. Weinkauf, H.-C. Hege, and H.-P. Seidel. On the applicability of topological methods for complex flow data. In H. Hauser, H. Hagen, and H. Theisel, editors, *Topology-based Methods in Visualization*, Mathematics and Visualization, pages 105–120. Springer, 2007. Topo-In-Vis 2005, Budmerice, Slovakia, September 29 - 30.

[39] H. Theisel, T. Weinkauf, H.-P. Seidel, and H. Seidel. Grid-Independent Detection of Closed Stream Lines in 2D Vector Fields. In *Proceedings of the Conference on Vision, Modeling and Visualization 2004 (VMV 04)*, pages 421–428, Nov. 2004.

[40] X. Tricoche, G. Scheuermann, and H. Hagen. Continuous topology simplification of planar vector fields. In *Proceedings of IEEE Visualization 2001*, pages 159–166, 2001.

[41] T. Weinkauf, H. Theisel, K. Shi, H.-C. Hege, and H.-P. Seidel. Extracting higher order critical points and topological simplification of 3d vector fields. In *Visualization, 2005. VIS 05. IEEE*, pages 559–566, Oct. 2005.

[42] T. Wischgoll and G. Scheuermann. Detection and Visualization of Closed Streamlines in Planar Fields. *IEEE Transactions on Visualization and Computer Graphics*, 7(2):165–172, 2001.

[43] T. Wischgoll and G. Scheuermann. Locating Closed Streamlines in 3D Vector Fields. In *Proceedings of the Joint Eurographics - IEEE TCVG Symposium on Visualization (VisSym 02)*, pages 227–280, May 2002.

[44] T. Wischgoll, G. Scheuermann, and H. Hagen. Tracking Closed Streamlines in Time Dependent Planar Flows. In *Proceedings of the Vision Modeling and Visualization Conference 2001 (VMV 01)*, pages 447–454, Nov. 2001.